SUPPLEMENTARY APPENDIX

Recapitulation of erythropoiesis in congenital dyserythropoietic anemia type I (CDA-I) identifies defects in differentiation and nucleolar abnormalities

Caroline Scott,[1] Damien J. Downes,[1] Jill M. Brown,[1] Robert A. Beagrie,[1] Aude-Anais Olijnik,[1] Matthew Gosden,[1] Ron Schwessinger,[1] Christopher A. Fisher,[1] Anna Rose,[1] David J.P Ferguson,[2] Errin Johnson,[3] Quentin A. Hill,[4] Steven Okoli,[5] Raffaele Renella,[6] Kate Ryan,[7] Marjorie Brand,[8] Jim Hughes,[1] Noemi B.A. Roy,[9,10] Douglas R. Higgs,[10] Christian Babbs[1] and Veronica J. Buckle[1]

[1]MRC Weatherall Institute of Molecular Medicine, Oxford University, Oxford, UK; [2]Ultrastructural Morphology Group, NDCLS, John Radcliffe Hospital, Oxford, UK; [3]Sir William Dunn School of Pathology, Oxford University, Oxford, UK; [4]Leeds Teaching Hospital NHS Trust, Leeds, UK; [5]Imperial College, The Commonwealth Building, The Hammersmith Hospital, Du Cane Rd, London, UK; [6]Pediatric Hematology-Oncology Research Laboratory, CHUV-UNIL Lausanne, Lausanne, Switzerland; [7]Department of Hematology, Manchester Royal Infirmary, Manchester, UK; [8]Sprott Center for Stem Cell Research, Ottawa Hospital Research Institute, Ottawa, Ontario, Canada; [9]Department of Hematology, Oxford University Hospitals NHS Trust, Churchill Hospital, Headington, and NIHR Biomedical Research Centre, Oxford, UK and [10]National Institute of Health Research Oxford Biomedical Research Center, Oxford, UK

 doi:10.3324/haematol.2020.260158

Received: May 20, 2020.

Accepted: September 17, 2020.

Pre-published: October 29, 2020.

Correspondence: *CAROLINE SCOTT* - caroline.scott@imm.ox.ac.uk

VERONICA BUCKLE - veronica.buckle@imm.ox.ac.uk

Recapitulation of erythropoiesis in congenital dyserythropoietic anaemia type I (CDA-I) identifies defects in differentiation and nucleolar abnormalities

Supplemental Data

Caroline Scott[1], Damien J. Downes[1], Jill M. Brown[1], Robert Beagrie[1], Aude-Anais Olijnik[1], Matthew Gosden[1], Ron Schwessinger[1], Christopher A. Fisher[1], Anna Rose[1], David J.P Ferguson[2], Errin Johnson[3], Quentin A. Hill[4], Steven Okoli[5], Raffaele Renella[6], Kate Ryan[7], Marjorie Brand[8], Jim Hughes[1], Noemi B.A. Roy[9], Douglas R. Higgs[1], Christian Babbs[1] and Veronica J. Buckle[1].

[1]Weatherall Institute of Molecular Medicine, Oxford University, Oxford, United Kingdom; [2]Ultrastructural Morphology Group, NDCLS, John Radcliffe Hospital, Oxford, United Kingdom; [3]Sir William Dunn School of Pathology, South Parks Rd, Oxford, United Kingdom; [4]Leeds Teaching Hospital NHS Trust, United Kingdom; [5]Imperial College, The Commonwealth Building, The Hammersmith Hospital, Du Cane Rd, London, United Kingdom; [6]Pediatric Hematology-Oncology Research Laboratory, CHUV-UNIL Lausanne Switzerland; [7]Department of Haematology, Manchester Royal Infirmary, Oxford Rd, Manchester, United Kingdom; [8]Sprott Center for Stem Cell Research, Ottawa Hospital Research Institute, Ottawa, Canada and [9]Department of Haematology, Oxford University Hospitals NHS Trust, Churchill Hospital, Old Rd, Headington, and NIHR Biomedical Research Centre, Oxford, United Kingdom.

Supplemental Figures

Supplemental Figure 1

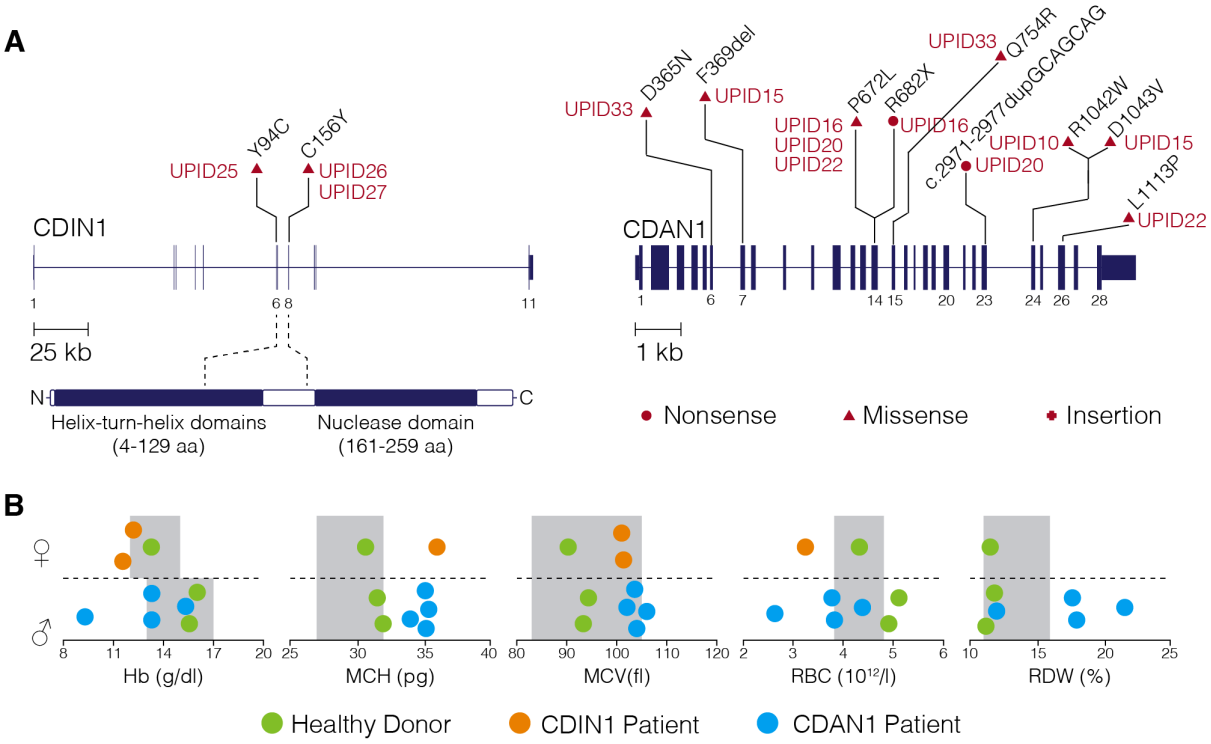

Supplemental Figure 1. CDA-I patient mutations and clinical data. (A) The location of pathogenic mutations associated with *CDIN1* and *CDAN1* of patients used in this study. Each patient has been given a unique personal identifier (UPID) and the type of mutation indicated. (B) Haematology of healthy donors (green dots) CDA-I patients with *CDIN1* mutations (orange dots) and with *CDAN1* mutations (blue dots) where full blood counts available. Grey boxes represent the Oxford University Hospital, NHS Foundation Trust normal ranges for adults. The gender of our cohort is also indicated. Haemoglobin (Hb), mean cell haemoglobin (MCH), mean cell volume (MCV), red blood cell count (RBC) and red cell distribution width (RDW). Data for UPID22 and UPID25 were omitted due to patients being venesected and transfused, respectively. For UPID10, 26 and 33 incomplete data were available.

Supplemental Figure 2

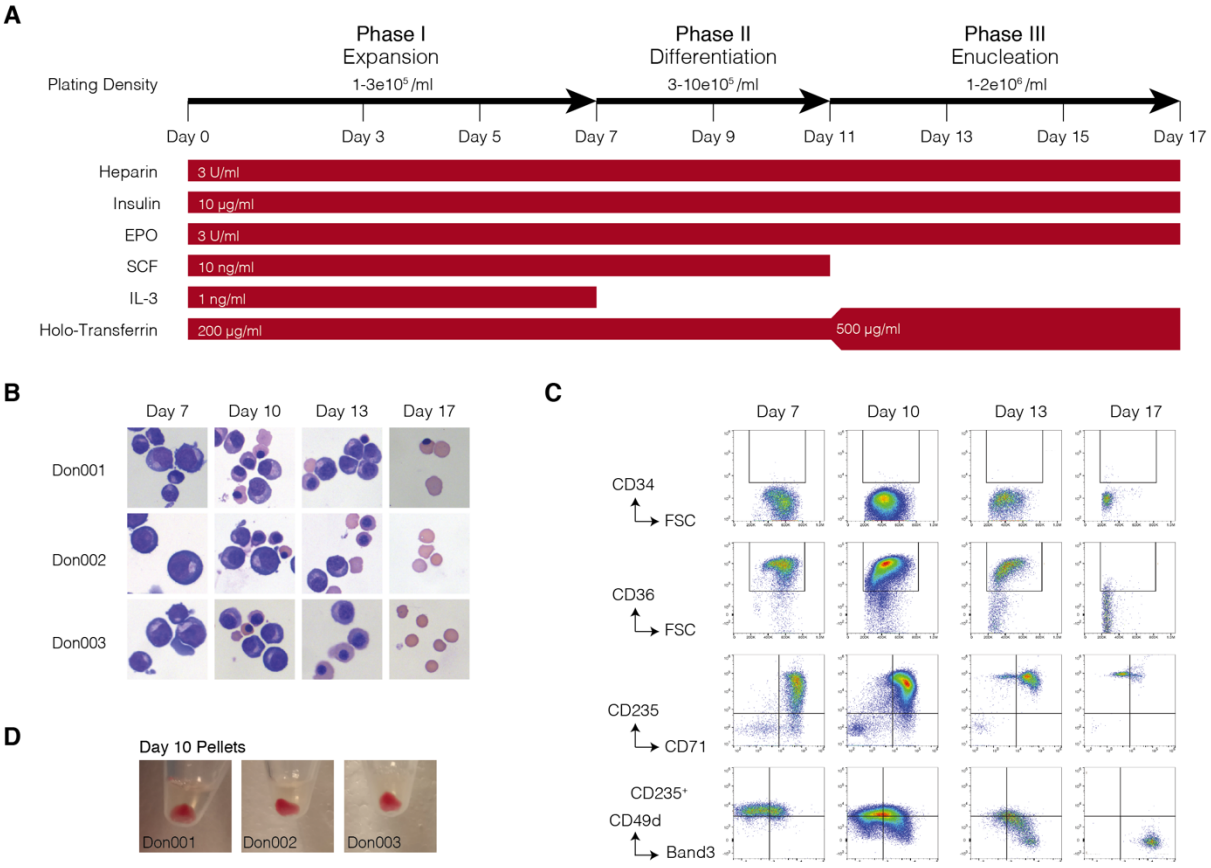

Supplemental Figure 2. Characterisation of protocol for expansion and differentiation of CD34⁺HSPCs from healthy donors. (A) Schematic of experimental approach for three-phase culture protocol. A common base media IMDM (Source BioScience UK Ltd) containing 3% (v/v) AB Serum, 10 µg mL-^{1}, insulin, 3 U mL-^{1} heparin (all from Sigma-Aldrich, Poole, UK), 2% (v/v) fetal bovine serum (Gibco) was supplemented as shown. (B) Representative cytospins stained with modified Wright's stain (magnification 40x) showing cell morphology during erythroid expansion (day 7), differentiation (day 10 and 13) and enucleation (day 17). (C) Immunophenotyping of cultured erythroblasts from peripheral blood of healthy donors (n=3) using a 6-colour antibody panel at days 7, 10, 13 & 17 of differentiation. Gates were set using fluorescence minus one (FMO) controls (see Supplemental Fig 3). (D) Images of red cell pellets from day 10 cultured erythroblasts.

Supplemental Figure 3

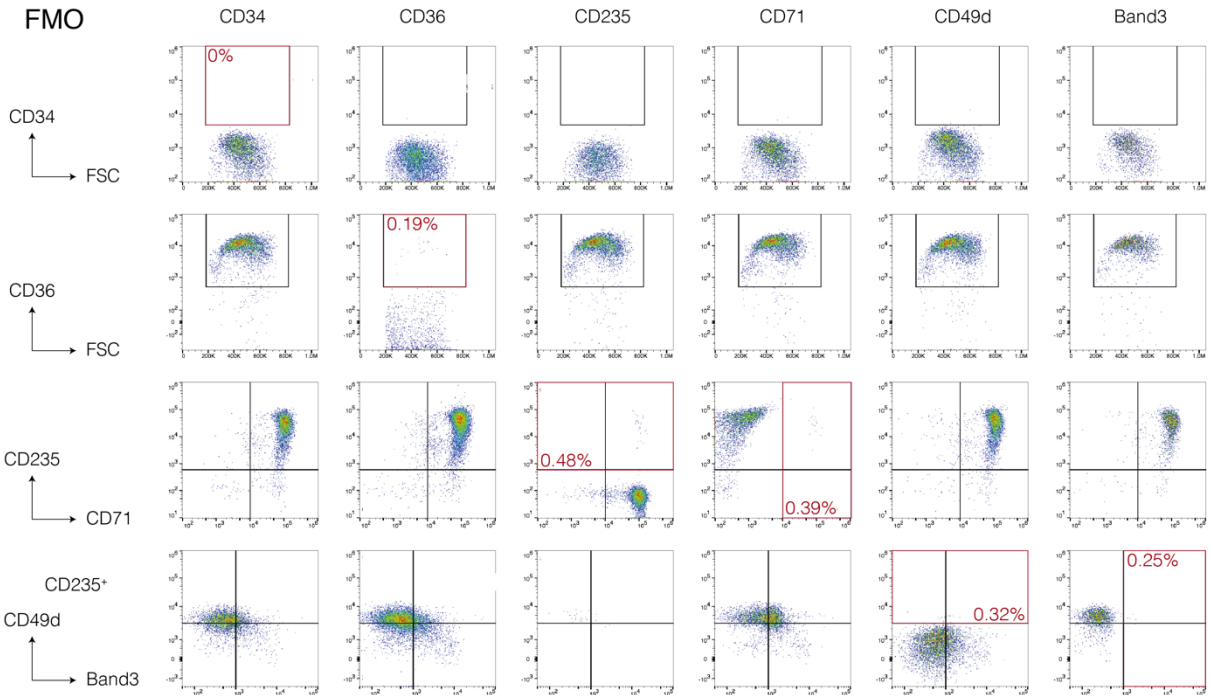

Supplemental Figure 3. Fluorescence minus one (FMO) controls for FACS analysis. Gating strategy for FACS analysis using FlowJo v10.4.2. Gates were set for each population on FMO. Red boxes indicated positive population for each marker and its relative percentage.

Supplemental Figure 4

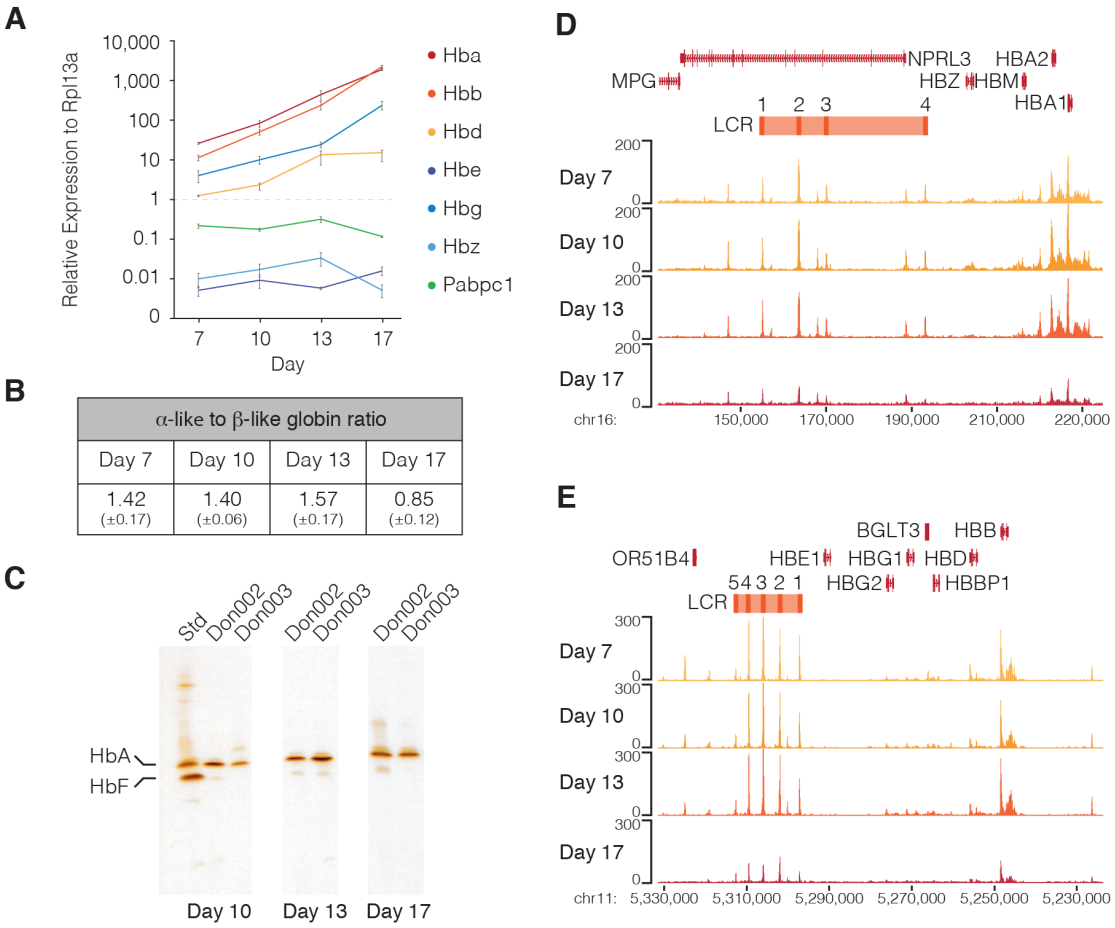

Supplemental Figure 4. Cultured erythroblasts from healthy donors show an increase in DNA accessibility and expression of the adult globin genes during differentiation. (A) RNA expression analysis of globins (mean ± SEM), throughout the differentiation normalized to RPL13A. Pabpc1 was used as a housekeeping gene. (B) Ratios of the alpha-like to beta-like globins (mean ± SEM) during erythroid differentiation. (C) IEF of erythroblasts from 2 healthy donors (Don002 and Don003) at three timepoints during *ex vivo* differentiation. HbA is adult haemoglobin and HbF is fetal haemoglobin. (D) ATAC-seq of the alpha-globin locus at four time-points throughout *ex vivo* differentiation of healthy controls (n=3, with technical replicates). (E) ATAC-seq of the beta-globin locus at four time-points throughout *ex vivo* differentiation of healthy controls (n=3, with technical replicates).

Supplemental Figure 5

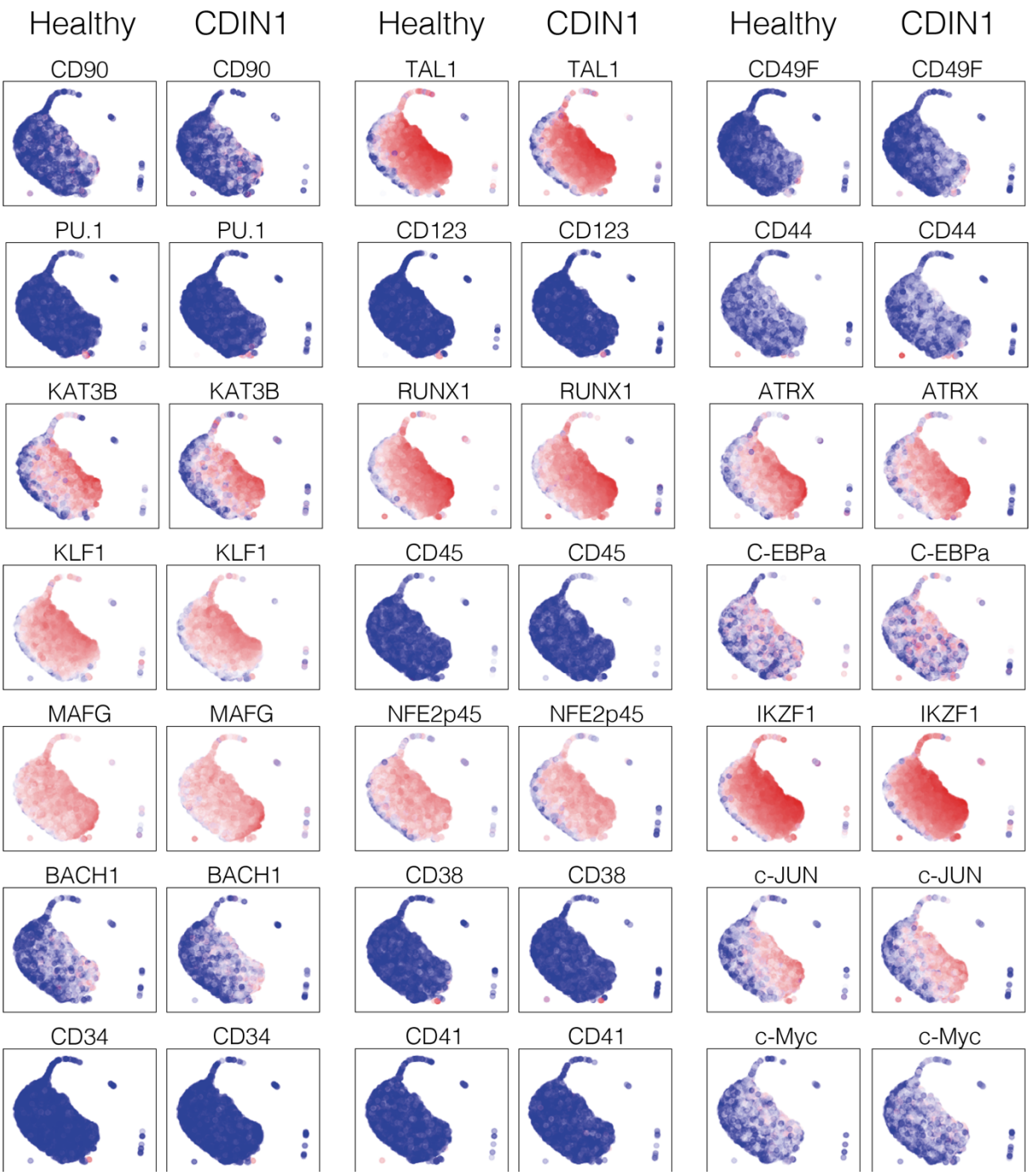

Supplemental Figure 5. UMAP plots of CyTOF data from day 11 cultured erythroblasts. UMAP plots showing the panel of CyTOF markers (Supplemental Table 6) analysed from healthy donors (n=3) and *CDIN1*-patient derived erythroblasts (n=3) at day 11 of differentiation. Plots are graded by colour from minimum (blue) to maximum (red) signal intensity. UMAP plots for CD235, CD71, CD36 and GATA1 shown in Figure 1B.

Supplemental Figure 6

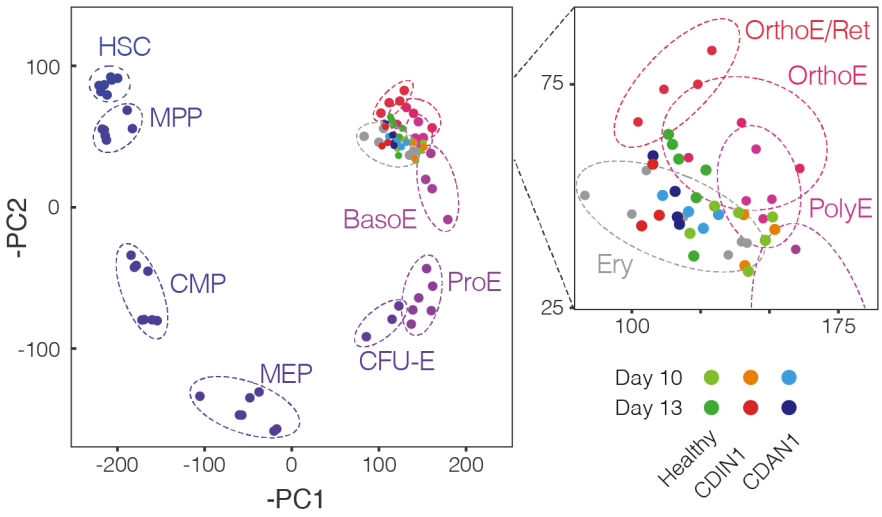

Supplemental Figure 6. DNA accessibility for CDA-I patient and healthy donor cultured erythroblasts mapped against a trajectory for normal erythropoiesis. PCA comparison of ATAC-seq for *ex vivo* differentiated erythroblasts from CDA-I patients (*CDIN1* patients n=3 and CDAN1 patients n=4) and healthy donors (n=6) using a trajectory of immunophenotyped sorted cell-types shows a clear overlap between groups. PCA was performed using 136698 peaks from haematopoietic stem cells (HSC), multi-potent progenitors (MPP), common myeloid progenitors (CMP), myeloid-erythroid progenitors (MEP) and bulk erythrocytes (Ery) from bone marrow or peripheral blood[1] and erythroid colony forming units (CFU-E), pro-erythroblasts (ProE), basophilic erythroblasts (BasoE), polychromatic erythroblasts (PolyE), orthochromatic erythroblasts (OrthoE) and reticulocytes (Ret) from *ex vivo* culture.[2] Healthy and CDA-I patient counts for PC1 and PC2 were then calculated and mapped relevant to the sorted populations.

Supplemental Figure 7

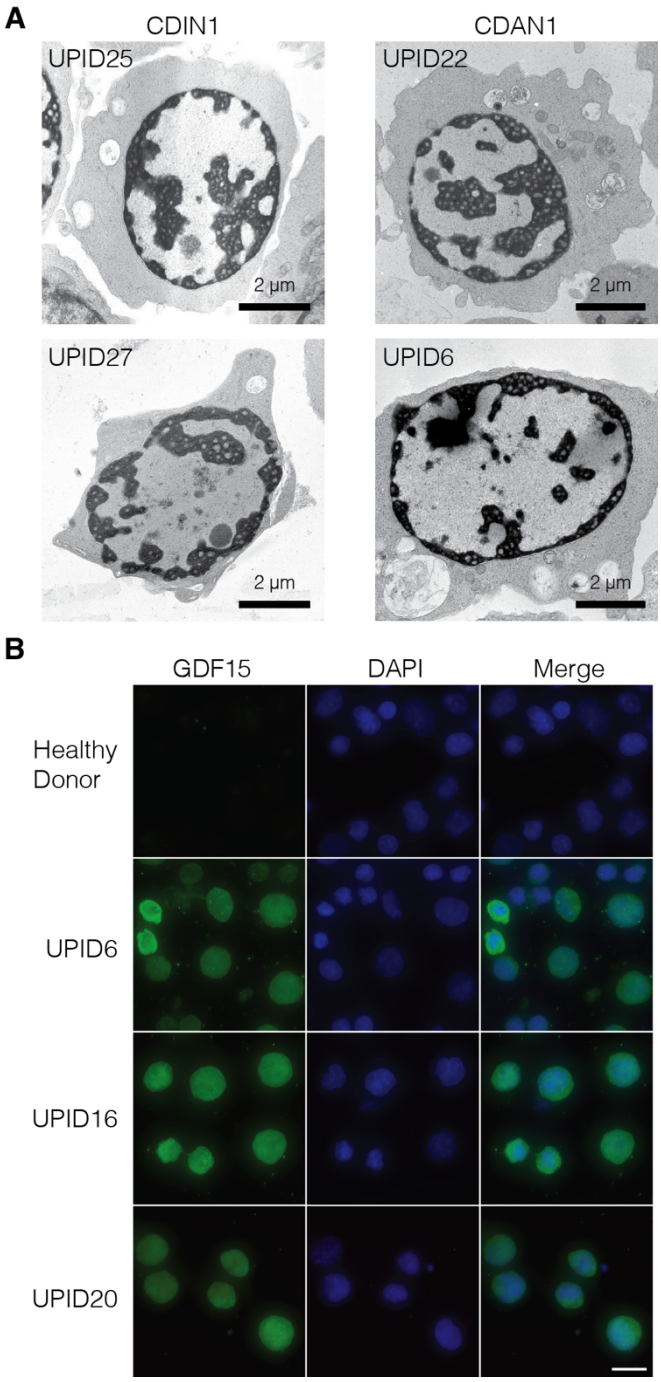

Supplemental Figure 7. *Ex vivo* cultured patient erythroblasts show the diagnostic features of CDA-I. (A) Representative examples of electron micrographs of abnormal nuclei seen in patients with mutations in *CDIN1* (n=2) and *CDAN1* (n=2). (B) Immunofluorescence of day 10 cultured erythroblasts from a healthy donor and *CDAN1* patients (UPID6, 16 and 20). GDF15 is detected with Alexa488 and DAPI was used as a nuclear counter stain. The merged images are shown in the right-hand panel. Bar is 8µm.

Supplemental Fig 8

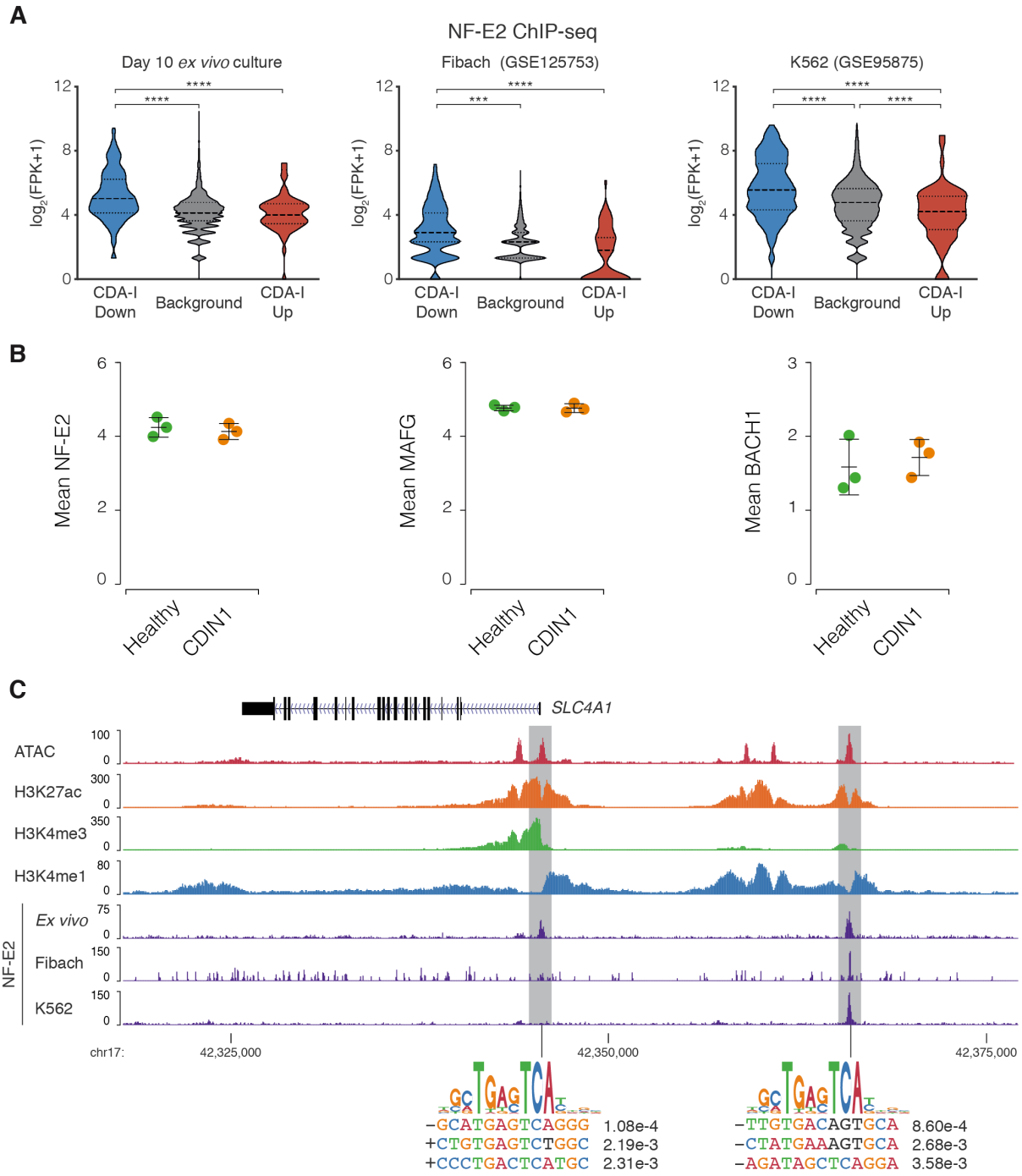

Supplemental Fig 8. NF-E2 regulation of differentially accessible peaks and Band 3. A) Counts of NF-E2 ChIP-seq reads over ATAC-seq peaks that had decreased accessibility (n=531), unchanged accessibility (n=3,742), or increased accessibility (n=61) in CDA-I patients. ChIP-seq is from day 10 *ex vivo* differentiation of CD34^{+} HSPCs, erythroblasts generated from peripheral blood mononuclear cells using the Fibach method[3] (GSE125753), and erythroleukemia K562 cells (GSE95875). Adjusted p-values (**** p<0.0001, *** p =0.001) are from a Kruskal-

Wallis test with Dunn's multiple comparison test correction show significantly more NF-E2 at open chromatin peaks with decreased accessibility in CDA-I patients. FPK: Fragments per kilobase. B) Mean CyTOF signal for the two protein components of NF-E2 (NFE2-p45 and MAFG) and for the transcription factor BACH1 (which binds to the same motif) at day 11 of *ex vivo* differentiation of healthy donor (n=3) and CDIN1 patient (n=3) $CD34^+$ HSPCs. Bars show mean and one standard deviation. C) Chromatin landscape at the Band 3 encoding gene, *Slc4a1*, at day 10 of *ex vivo* differentiation from healthy donors, showing open chromatin (ATAC), promoter sites (H3K4me3), enhancers (H3K4me1), active transcription (H3K27ac) and NF-E2 binding. NF-E2 signal is also shown from Fibach and K562 erythroid cells. Grey bars highlight the NF-E2 bound peaks (promoter left and 5' enhancer right) with motif analysis below. P-values for FIMO comparison with NFE2_HUMAN.H11MO.0.A are shown.

Supplemental Figure 9

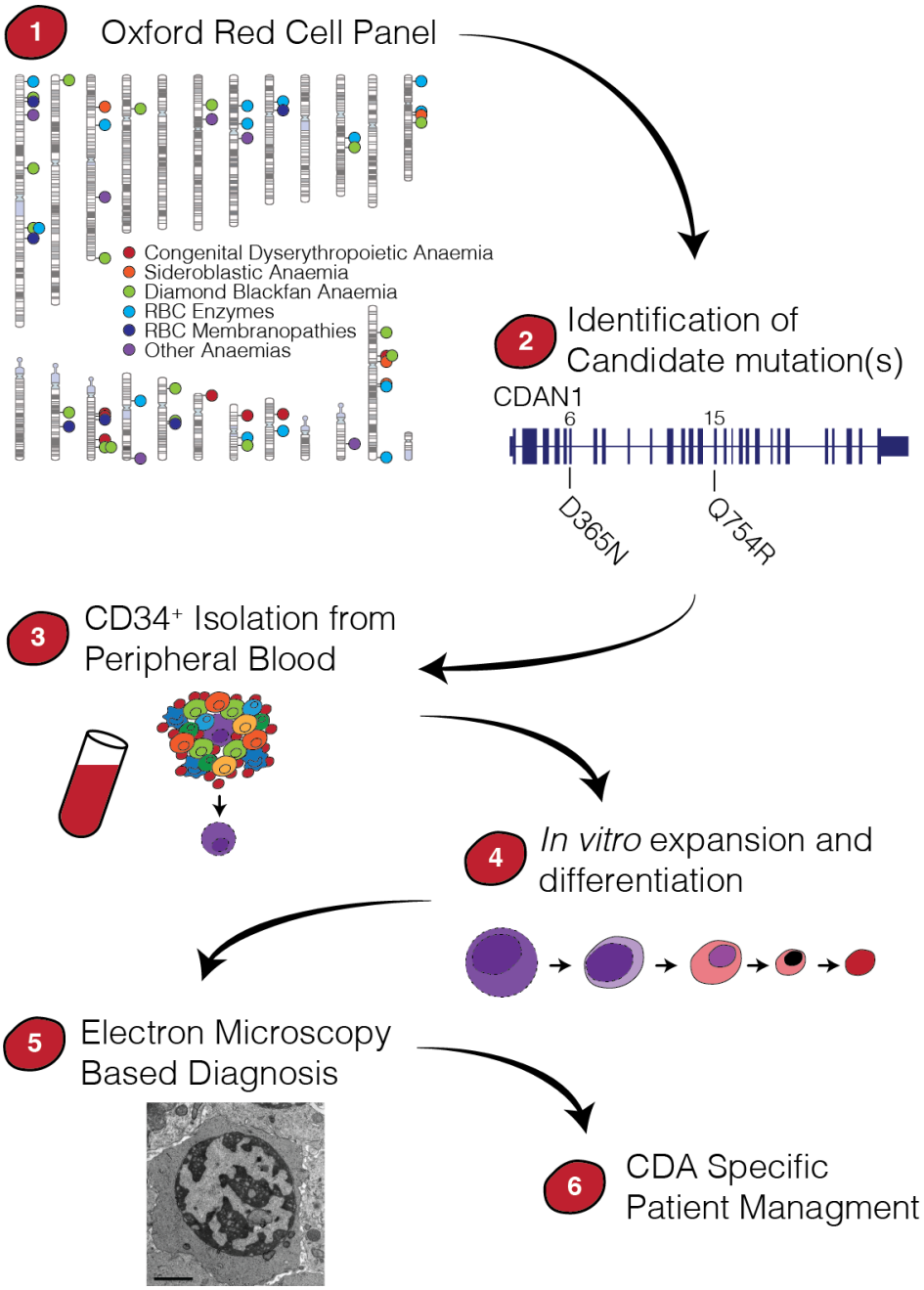

Supplemental Figure 9. Strategy for generation of patient specific erythroblasts to validate CDA-I variants. Mutations in *CDAN1* genes were identified from gDNA of patient peripheral blood (UPID33) using a targeted re-sequencing Oxford Red Cell Panel[4] and validated by demonstrating the presence of 'spongy' heterochromatin in *ex vivo* cultured erythroblasts, thus confirming the diagnosis of CDA-I.

Supplemental Figure 10

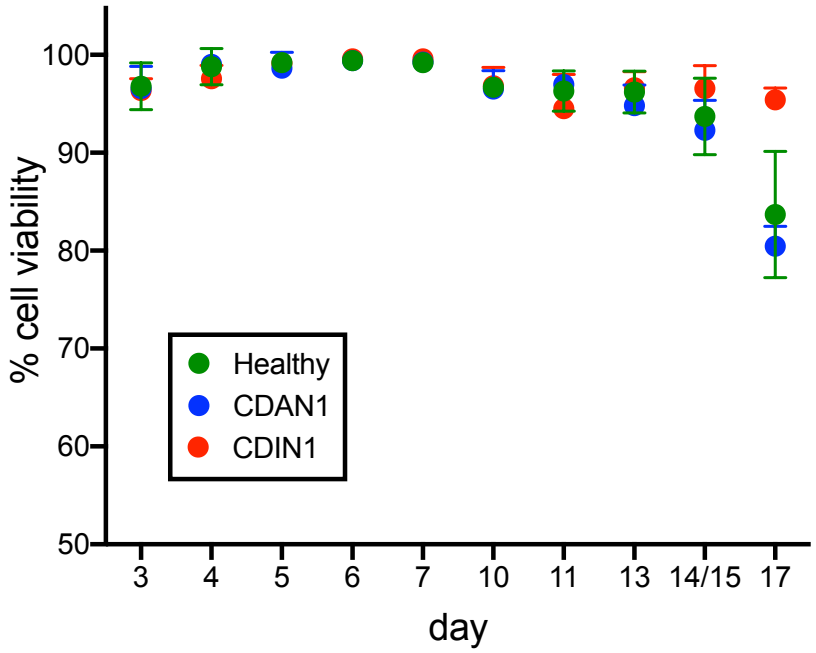

Supplemental Figure 10. Cell viability during *ex vivo* culture period. Daily viability scores for *ex vivo* cultures from healthy donors (n=11) and CDA-I patients with mutations in *CDAN1* (n=6) or *CDIN1* (n=5), measured by staining with acridine orange and DAPI.

Supplemental Tables

Supplemental Table 1. Fluorophore conjugated antibodies used for staging the erythroid differentiation by FACS.

	Protein	Channel	Supplier	Catalogue Number
CD235a	Glycophorin A	PE	BD Bioscience	555570
CD71	Transferrin receptor	PerCP Cy5.5	Biolegend	334114
CD49D	α-Integrin	APC	BD Bioscience	561892
CD34	CD34	PE/Cy7	Biolegend	343616
CD233	Band3	FITC	IBGRL	9439FI
CD36	Platelet glycoprotein	APC/Cy7	Biolegend	336213
Hoechst 33258	Viability dye	Violet	Invitrogen	H3569

Supplemental Table 2: TaqMan probes used for globin expression analysis.

Gene	Product Code
HBA	Hs00361191_g1
HBB	Hs00747223_g1
HBD	Hs00426283_m1
HBE	Hs00362216_m1
HBG	Hs00361131_g1
HBZ	Hs00923579_m1
RPL13a	Hs03043885_g1
PABPC1	Hs00743792_s1

Supplemental Table 3: Next generation sequencing depth. See file designated 'Supplemental Excel Tables'.

Supplemental Table 4: Bed file of top 1000 ATAC peaks used for PCA plots. See file designated 'Supplemental Excel Tables'.

Supplemental Table 5: Bed file of ATAC-seq non-TSS nucleosome depleted regions (NDR) used for PCA plots. See file designated 'Supplemental Excel Tables'.

Supplemental Table 6: Pre-conjugated antibodies used for CyTOF.

Label	Antibody Target	Clone	Source	Catalog number	RRID
149Sm	CD34	581	Fluidigm	3149013B	AB_2756285
155Gd	CD36	5-271	Fluidigm	3155012B	AB_2756286
175Lu	CD71	OKT-9	Fluidigm	3175011B	AB_2756287
172Yb	CD38	HIT2	Fluidigm	3172007B	AB_2756288

143Nd	CD45RA	HI100	Fluidigm	3143006B	AB_2651156
151Eu	CD123	6H6	Fluidigm	3151001B	AB_2661794
164Dy	CD49F	G0H3	Fluidigm	3164006B	AB_2756289
161Dy	CD90	5E10	Fluidigm	3161009B	AB_2756290
153Eu	CD44	691534	Fluidigm	3153021B	AB_2756291
89Y	CD41	HIP8	Fluidigm	3089004B	AB_2756292
141Pr	CD235ab	HIR2	Fluidigm	3141001B	AB_2651154
PE	GATA1	234739	R&D Systems	C1779P	AB_2108404
156Gd*	A-PE	PE001	Fluidigm	3156005B	AB_2756294
167Er	PU1	7C6B05	Biolegend	658002	AB_2562720
160Gd	ATRX	39f	Abcam	218936	AB_2756295
176Yb	c-Myc	9E10	Fluidigm	3176012B	AB_2756296
165Ho	KLF1	1B6A3	Abcam	175372	AB_2756297
162Dy	TAL1	2TL242	Thermo	14-9101-82	AB_2572922
158Gd	RUNX1	polyclonal	Thermo	PA5-12409	AB_2184103
154Sm	NFE2p45	polyclonal	Genetex	GTX102698	AB_1950992
171Yb	BACH1	GO11-1A3	Thermo	37-0900	AB_2533297
159Tb	IKZF1	polyclonal	Thermo	PA5-23728	AB_2541228
152Sm	MAFG	polyclonal	Genetex	GTX114541	AB_10619599
173Yb	c-JUN	2HCLC	Thermo	711202	AB_2633131
166Er	KAT3B/p300	RW105	Novusbio	NB100-616	AB_10002598
145Nd	C/EBPa	polyclonal	Thermo	PA5-26487	AB_2543987

*this antibody was used as a secondary antibody to detect the PE-labelled GATA1 antibody

Supplemental Table 7: Antibodies used for IF.

Antibody	**Source**	**Dilution**
goat anti-GDF15	ab-39999; Abcam	1:50
anti–goat Alexa488	A-11055; Thermo Fisher Scientific	1:300
rabbit anti-Codanin-1	Bethyl A304-951A	1:300
rabbit anti-C15orf41	Cusabio CSB-PA897474LA01HU	1:50
mouse anti-Fibrillarin	Abcam ab4566	1:500
mouse anti-UBF	Santa Cruz F-9	1:100

donkey anti-mouse Cy3	Jackson Immunoresearch	1:500
donkey anti-rabbit Alexa 488	ThermoFisher Scientific	1:200

Supplemental Table 8: CDA-I patient mutations and disease severity

Patient ID	Gender	Age (yrs)	Gene	Mutation types	Disease severity
UPID6	M	54	*CDAN1*	Unknown effect	mild
UPID10	M	46	*CDAN1*	Non LOF	moderate
UPID15	M	70	*CDAN1*	Unknown effect/Non LOF	mild
UPID16	M	50	*CDAN1*	LOF/Non LOF	mild
UPID20	M	72	*CDAN1*	LOF/Non LOF	mild
UPID22	F	30	*CDAN1*	Non LOF/Unknown effect	moderate
UPID33	M	8	*CDAN1*	Unknown effect/Unknown effect	severe
UPID25	F	46	*CDIN1*	Unknown effect	severe
UPID26	F	46	*CDIN1*	Unknown effect	mild
UPID27	F	42	*CDIN1*	Unknown effect	mild

Supplemental Methods

Differentiation of CD34$^+$ HSPCs: 1x10^5 cells were resuspended on day 0 in Phase I media (see Supplemental Figure 2A) at 10^5 cells ml^{-1}. Cell counts and viability was assessed throughout the differentiation using the cell count and viability assay on the Nucleocounter 3000 (Chemometec). Acridine orange was used to stain the entire population, DAPI to stain the non-viable cells and % viability calculated from these. On days 3 and 5 with additional Phase I media the cell concentration was maintained at 2x10^5 cells ml^{-1}. On day 7, cells were counted and pelleted (400 rcf, 5 min, RT) and resuspended in Phase II media at 2x10^5 cells ml^{-1}. Cells were counted on day 9 and diluted to 2x10^5 cells ml^{-1} Phase II media. On day 11, cells were counted and pelleted (400 rcf, 5 min, RT) and resuspended in Phase III media at 1x10^6 cells ml^{-1}. Cells were counted on days 13 and 15 and diluted to 1x10^6 cells ml^{-1} in Phase III media. Live cell counts were normalized to 1x10^5 cells ml^{-1} on day 5 to take into account different numbers of starting cells after freezing. The Mann-Whitney rank sum test with Benjamini-Hochberg multiple test correction ($q<0.05$) was used to compare cell counts of healthy and CDA-I patient samples.

Morphological analysis using Cytospins: 1x10^5 cells were resuspended in 200 μL PBS, spun (5min, 400 rpm) in a Cytospin4 (ThermoFisher), stained with modified Wright's stain and mounted in DPX (Sigma). Cytospins were imaged using an Olympus BX60 microscope with10x and 20x objectives. Using images of the cytospins, the morphology of the cultured erythroblasts was scored with the following categories; pro-erythroblasts (Pro), basophilic erythroblasts (Baso), polychromatic erythroblasts (Poly), orthochromatic erythroblasts (Ortho) and enucleated (Enuc).

Iso-electric Focusing: 1x10^6 cultured erythroblasts were lysed in Haemoglobin elution solution and 50% loaded on an iso-electric focusing (IEF) gel (RESOLVE® Haemoglobin kit, PerkinElmer, USA) then run at 1200v for 90min at 15^{o}C on a water-cooled horizontal electrophoresis rig (GE Healthcare). Gels were fixed in 10% trichloroacetic acid and stained with the JB-2 system (Perkin Elmer, USA) as per manufacturer instructions.

CyTOF: CyTOF detects expression levels of multiple proteins in single cells by staining with antibodies conjugated to heavy metal isotopes. Levels of each isotope

are measured by mass spectrometry which eliminates the problem of spectral overlap associated with FACS and thus expands the parameters that can be measured simultaneously.

ATAC-Seq Library preparation and analysis: Immunoprecipitated material was indexed using NEB Next Ultra II DNA library prep kit for Illumina (New England Biolabs). ChIP-seq and ATAC-seq libraries were sequenced on the NextSeq platform (Illumina v2 chemistry) with 39-bp paired-end reads. Reads were mapped to the hg19genome using NGseqBasic[5] (V20; --nextera --blacklistFilter --noWindow), which utilises Bowtie.[6] Sequence depth and mapped reads are provided (Supplemental Table 3). GEO repositories of sorted cell population ATAC-seq (GSE75384, GSE115684),[1, 2] chromatin marks (GSE125926)[7] and NF-E2 ChIP-seq (GSE125753, GSE95875)[8] (ENCODE) were analysed by the same method. For visualisation PCR-duplicate filtered replicates were merged using Samtools[9] (v1.3) and converted to bigwig format with minimal smoothing using deepTools[10] (v2.2.2; bamCoverage --binSize 10 --normalize using RPKM). ATAC-seq peaks were called from sorted hematopoietic populations (Supplemental Tables 4 and 5), healthy donor and patient samples using Macs2[11] (v2.0/10 callpeak -f BAMPE -g 1.87e9 -q 0.1). Peaks identified in less than three samples were discarded and remaining peaks were merged using BEDtools merge[12] (v2.25.0), to form a collection of peaks detected across all cell types. For differentiation trajectory plotting, principal component analysis (PCA) was performed on published datasets using scikitlearn (v0.22), then samples from *ex vivo* differentiation cultures were projected into the same space using the rotation identified from purified subpopulations. Differential accessibility was determined using DESeq2[13] by comparing ATAC-seq read counts in autosomal open chromatin regions from both day 10 and day 13 from two separate differentiations of three healthy donors (n=6 for each timepoint) with CDA-I patients comprised of both *CDIN1* patients (n=3 for each timepoint) and *CDAN1* patients (n=4 for each timepoint). A factorial design was used to account for changes between day 10 and day 13 as well as changes between CDA-I patients and healthy donors. Motif identification was performed using MEME, using a custom background of peaks that were accessible in *ex vivo* cultured cells but which maintained the same accessibility between CDA-I patients and healthy donors.[14]

Immunofluorescence (IF): 1-2x10^5 cells were washed and settled on poly-L-lysine treated coverslips (5 mins). Cells were fixed (4% PFA, 15 min) and permeabilized in 0.2% Triton X100 in PBS (10 min, RT). Slides were blocked using 10% FCS in PBS (RT for 30 mins). Antibodies were prepared in blocking solution (Supplemental Table 7). Following detection, slides were washed in PBS, fixed (4% PFA) and coverslips mounted in Vectashield with 1 μg mL^{-1} DAPI added as a nuclear counterstain.

Fluorescence in situ hybridization (FISH): Cells were washed in PBS, settled on clean poly-l-lysine coated slides for 5 min, then slid horizontally into a dish containing 3:1 (vol:vol) methanol : acetic acid fixative for 10 min. Following fixation slides were dried vertically and stored at -20 °C with desiccant. To perform FISH, slides were treated with 100 μg/ mL RNase at 37 °C for 1 hr, washed in 2xSSC, dehydrated through an ethanol series, denatured in 70% formamide in 2xSSC pH 7.0 at 74 °C for 5 min, dehydrated through an ice-cold ethanol series and air-dried. Labelled probes (100 ng each) were denatured in hybridization buffer (Leica, KBI-FHB) at 90 °C for 10 min; BACs were preannealed at 37 °C for 20 min. Slides were hybridized with prepared probes at 37 °C overnight. After hybridization, slides were washed as follows; 2 min in 2xSSC with 0.1% IGEPAL® CA 630 (vol/vol) to remove coverslips, 2 min 2xSSC with 0.1% IGEPAL® CA 630 (vol/vol), then 2 min exactly at 70 °C in 0.4x SSC with 0.3% IGEPAL® CA 630 (vol/vol). Following 1 min in 2xSSC with 0.1% IGEPAL® CA 630 (vol/vol), slides were blocked in 3% BSA (wt/vol) in 4xSSC and digoxigenin was detected with sheep anti-digoxigenin FITC 1:50 (Roche, 11207741910) followed by rabbit anti–sheep FITC 1:100 (Vector Laboratories, FI-6000). Slides were mounted in Vectashield (Vector Laboratories) containing 2 μg/ mL DAPI.

Imaging equipment, settings and image restoration: Widefield fluorescence imaging was performed at 20 °C on a DeltaVision Elite system (Applied Precision) using a 100 ×/1.40 NA UPLSAPO oil immersion objective for FISH slides and a 60x/1.42 NA PLAPON oil immersion objective (Olympus) for immunofluorescence, a CoolSnap HQ2 CCD camera (Photometrics), DAPI (excitation 390/18; emission 435/40), FITC (excitation 475/28; emission 525/45) and TRITC (excitation 542/27; emission 593/45) filters. 12-bit image stacks were acquired with a z-step of 200 nm giving a voxel size of 64.5 nm x 64.5 nm x 200 nm (x100 objective) or 108.2 nm x 108.2 nm x200 nm (x60 objective). For the immunofluorescence shown in Figure 6C, image restoration was

carried out using Huygens deconvolution Classic Maximum Likelihood Estimation (Scientific Volume Imaging B.V.).

Supplemental References

1. Corces MR, Buenrostro JD, Wu B, et al. Lineage-specific and single-cell chromatin accessibility charts human hematopoiesis and leukemia evolution. Nat Genet. 2016;48(10):1193-1203.
2. Ludwig LS, Lareau CA, Bao EL, et al. Transcriptional States and Chromatin Accessibility Underlying Human Erythropoiesis. Cell Rep. 2019;27(11):3228-3240 e3227.
3. Fibach E, Manor D, Oppenheim A, Rachmilewitz EA. Proliferation and maturation of human erythroid progenitors in liquid culture. Blood. 1989;73(1):100-103.
4. Roy NB, Wilson EA, Henderson S, et al. A novel 33-Gene targeted resequencing panel provides accurate, clinical-grade diagnosis and improves patient management for rare inherited anaemias. Br J Haematol. 2016;175(2):318-330.
5. Telenius J, Hughes JR. NGseqBasic - a single-command UNIX tool for ATAC-seq, DNaseI-seq, Cut-and-Run, and ChIP-seq data mapping, high-resolution visualisation, and quality control. bioRxiv. 2018;393413.
6. Langmead B, Trapnell C, Pop M, Salzberg SL. Ultrafast and memory-efficient alignment of short DNA sequences to the human genome. Genome Biol. 2009;10(3):R25.
7. Downes DJ, Schwessinger R, Hill SJ, et al. An integrated platform to systematically identify causal variants and genes for polygenic human traits. bioRxiv. 2020;813618.
8. Olijnik AA, Roy NBA, Scott C, et al. Genetic and functional insights into CDA-I prevalence and pathogenesis. J Med Genet. 2020;in press.
9. Li H, Handsaker B, Wysoker A, et al. The Sequence Alignment/Map format and SAMtools. Bioinformatics. 2009;25(16):2078-2079.
10. Ramirez F, Ryan DP, Gruning B, et al. deepTools2: a next generation web server for deep-sequencing data analysis. Nucleic Acids Res. 2016;44(W1):W160-165.
11. Feng J, Liu T, Qin B, Zhang Y, Liu XS. Identifying ChIP-seq enrichment using MACS. Nat Protoc. 2012;7(9):1728-1740.
12. Quinlan AR, Hall IM. BEDTools: a flexible suite of utilities for comparing genomic features. Bioinformatics. 2010;26(6):841-842.
13. Love MI, Huber W, Anders S. Moderated estimation of fold change and dispersion for RNA-seq data with DESeq2. Genome Biol. 2014;15(12):550.
14. Bailey TL, Boden M, Buske FA, et al. MEME SUITE: tools for motif discovery and searching. Nucleic Acids Res. 2009;37(Web Server issue):W202-208.